Lattice dynamics investigation of different transition behaviors of cubic $BaTiO_3$ and $SrTiO_3$ by first-principles calculations

2008 J. Phys.: Condens. Matter 20 215215

(http://iopscience.iop.org/0953-8984/20/21/215215)

IOP PUBLISHING JOURNAL OF PHYSICS: CONDENSED MATTER

J. Phys.: Condens. Matter **20** (2008) 215215 (8pp) doi:10.1088/0953-8984/20/21/215215

Lattice dynamics investigation of different transition behaviors of cubic $BaTiO_3$ and $SrTiO_3$ by first-principles calculations

Ying Xie, Hai-tao Yu, Guo-xu Zhang and Hong-gang Fu[1]

Laboratory of Physical Chemistry, School of Chemistry and Materials Science, Heilongjiang University, Harbin 150080, People's Republic of China

E-mail: fuhg@vip.sina.com

Received 24 December 2007, in final form 13 March 2008
Published 22 April 2008
Online at stacks.iop.org/JPhysCM/20/215215

Abstract

The lattice dynamics of cubic $BaTiO_3$ and $SrTiO_3$ at different crystal lattice volumes were investigated using first-principles density functional theory calculation. The computational results indicate that the Ti–O and A–O (A = Sr or Ba) interactions are responsible for the unstable ferroelectric Γ_{15} and antiferrodistortive R_{25} phonons, respectively. With decreasing volume, the Γ_{15} phonon behaviors of cubic $SrTiO_3$ and $BaTiO_3$ show a similar trend and the Ti–O repulsions are significantly enhanced, leading to the disappearance of ferroelectric instability. However, for $BaTiO_3$ the large ionic radius of Ba with respect to Sr results in a repulsive Ba–O interaction and thereby the disappearance of the R_{25} instability, while the long-range characteristic of Sr–O pair are crucial for the antiferrodistortive instability of cubic $SrTiO_3$. By analyzing the real-space interatomic force constants, it can be confirmed that the different antiferrodistortive behaviors of the two compounds are dictated by different short-range repulsions of A–O pairs. Moreover, owing to the smaller ionic radius of Sr relative to Ba, the lattice constant of $SrTiO_3$ can be significantly reduced, leading to the absence of ferroelectric instability for $SrTiO_3$. The substitution and different crystal volumes make the phase transitions of the two compounds entirely different.

1. Introduction

The perovskites are an extremely important group of ferroelectric materials. Their importance stems not only from technological applications but also from fundamental interest in understanding structural phase transitions. Generally, the perovskites share a common ABO_3 formula and possess a highly symmetrical cubic structure. With decreasing temperature, they display a variety of phase transitions, ranging from non-polar antiferrodistortive (AFD) transition to ferroelectric (FE) and antiferroelectric (AFE) ones in nature [1].

Among the perovskite family, $BaTiO_3$ and $SrTiO_3$ are two widely used ceramics. However, they possess very different phase transition characteristics. $SrTiO_3$ behaves as an incipient ferroelectric and undergoes an AFD transition at 110 K [2], while $BaTiO_3$ exhibits a complicated sequence of FE phase transitions from cubic symmetry to tetragonal, orthorhombic, and rhombohedral structures [3]. Though much progress has been made in the experimental characterization of the properties of the two compounds during the past several decades [2–6], our knowledge concerning the nature of their phase transitions was rather limited until accurate first-principles density functional theory (DFT) calculations were employed to study the potential energy surfaces [7–10] and temperature-dependent phase diagrams [11–14] of various perovskite oxides in the last decade. These early theoretical works proved to be quite accurate in the prediction of ground-state structure and structural parameters of perovskites [9], giving us confidence to elucidate the microscopic behaviors, i.e. the origin of ferroelectricity [7, 8] and the competition between long-range and short-range (SR) interactions [8]. On the other hand, with advances in density functional perturbation theory (DFPT) [15], it is already feasible to analyze the transition behaviors of some compounds by computing their lattice dynamics by first-principles

[1] Author to whom any correspondence should be addressed.

methods [16–18]. Relying on the linearized augmented plane-wave method, Lasota and co-workers computed the full phonon dispersion relation of cubic $SrTiO_3$, by which they confirmed the AFD instability observed in a previous experiment [16]. To identify the effect of substitution on the lattice dynamics, Ghosez and co-workers calculated the phonon bands and interatomic force constants (IFCs) of $BaTiO_3$, $PbTiO_3$, and $PbZrO_3$ by the *ab initio* pseudopotential technique and confirmed that the A–O (A = Pb, Ba) and B–O (B = Ti, Zr) longitudinal interactions are responsible for the different transition behaviors of the three compounds [17]. Later, Trautmann and co-workers investigated the influences of dipole and charge fluctuations on the lattice dynamics of $SrTiO_3$ and $BaTiO_3$ and confirmed the effect of long-rang and SR interactions on the FE and AFD transition behaviors [18].

Despite many significant theoretical achievements in the past 10 years [7–14, 16–18], some problems still deserve our consideration. According to previous investigations, the hybridization between Ti_{3d} and O_{2p} states is essential for the ferroelectricity of $BaTiO_3$ and $PbTiO_3$ [8]. However, for $SrTiO_3$ the situation is very different. Though the Ti–O covalent bonding in $SrTiO_3$ can be confirmed to be similar to that in $BaTiO_3$ and $PbTiO_3$ [19], it is indubitable that $SrTiO_3$ undergoes an AFD transition but not a FE one [2]. To investigate the effect of A- and B-site ions on structural instabilities, Ghita and co-workers classified the perovskites into four types by different tolerance factors (t) and pointed out that $t < 1$ or $t = 1$ represent A-site driven instability (AFE instability, i.e. $PbZrO_3$) or a stable cubic phase (i.e. $BaZrO_3$), respectively, while $t > 1$ corresponds to B-site (i.e. $BaTiO_3$) and AB-site (i.e. $PbTiO_3$) driven ferroelectric instability [20]. Although this classification is quite predictive with regard to what pattern of instability will occur in a given material, how the ionic radius (related to the tolerance factor) affects the structural instabilities is still unclear. To this purpose, further investigations concerning the long-range and SR interaction of different ionic pairs are very necessary. Moreover, as well as the atoms at position A, the lattice constants of $BaTiO_3$ and $SrTiO_3$ are also different, and it is hard to identify which factor is responsible for their different transition behaviors. However, previous experimental investigations on $PbZrO_3$, PbH_fO_3, and $BaMnF_4$ compounds indicated that the FE instability is suppressed while the AFE instability is enhanced under external pressures [21, 22]. Further theoretical investigations on $KNbO_3$ [23] and $PbZr_xTi_{1-x}O_3$ [24] also support the above idea that FE and AFE instabilities show an opposite trend under hydrostatic pressures [23, 24]. Therefore, relevant discussions on the changed interaction of different ionic pairs under pressure are also helpful. With these points in mind, in this study we decided to calculate the Born effective charges (BECs), phonon dispersion relations, and IFCs of cubic $BaTiO_3$ and $SrTiO_3$ followed by examination of the effect of substitution and crystal volume change on the lattice dynamics to clarify the possible origin of their different transition behaviors.

2. Computational details

All calculations in present study were performed within the DFT framework [25] implemented in the ABINIT package [26, 27]. The local density approximation pseudopotentials used in calculations were generated by the Troullier–Martins scheme [28] with the FHI98PP code [29]. The exchange–correlation energy was evaluated by the Perdwe–Wang parametrization [30] of the Ceperley–Alder density functional [31]. The conjugate gradient method was employed to minimize the Kohn–Sham energy [32], and the plane-wave cutoff used is 45 Hartree. The sampling over the Brillouin zone was treated by a $(4 \times 4 \times 4)$ Monkhorst–Pack mesh [33].

The optical dielectric constants, BECs, and dynamical matrices were computed according to the DFPT method [15]. To correctly handle the long-range characteristics of the system, the dipole–dipole (DD) contribution was subtracted from the dynamical matrix in reciprocal space and calculated separately through the Ewald technique [34, 35]. Then, the SR contribution to the IFCs in real space was obtained from the remainder of the dynamical matrix by using the Fourier transform [34, 35]. Therefore, the IFC matrix $C_{\alpha,\beta}(lk,\ l'k')$, defined as $F_\alpha(lk) = -C_{\alpha,\beta}(lk,\ l'k')\Delta\tau_\beta(l'k')$, where $F_\alpha(lk)$ and $\Delta\tau_\beta(l'k')$ represent the force on atom k in cell l and the displacement of atom k' in cell l', respectively, can be determined. On the basis of the IFCs, the phonon dispersion bands were thus obtained by an elaborate Fourier interpolation. Moreover, to control the errors caused by the Fourier interpolation, a $2 \times 2 \times 2$ centered cubic mesh with a Γ point was used for computing the SR contribution from a dynamical matrix.

For cubic phase $SrTiO_3$ and $BaTiO_3$, the A (A = Sr, Ba), Ti, and O atoms are located at the corner, body center, and face center of the cubic lattice, respectively. In consideration of the substitution effect and different lattice volumes of the two compounds, we decided to calculate their lattice dynamics properties at different lattice constants to clarify the discrepancies of their phase transition behaviors.

3. Results and discussion

3.1. Effect of volume on dielectric properties

The computed optical dielectric constants (ε_∞), which are usually overestimated within the LDA scheme [16, 17], are presented in table 1. According to previous predictions, the errors of ε_∞ in cubic $SrTiO_3$ and $BaTiO_3$ are over 14% by comparing the theoretical values (6.63 and 6.75) [16, 17] with the experimental ones (5.83 and 5.40) [36, 37]. The origin of the error is very complex, and it arises at least partly from the lack of polarization dependence of the approximate exchange–correlation functional [38]. However, by selecting suitable parameters the calculation can be improved, as it is noted from table 2 that the optical dielectric constants, lattice constants, and Γ_{15} modes are obviously affected by the pseudopotentials and functionals used. In comparison with the experimental dielectric constants (5.83 and 5.40 for $SrTiO_3$ and $BaTiO_3$,

Table 1. Lattice parameters (Å) used in the DFPT calculations, BECs (Z^*, $|e|$), and optical dielectric constants (ε_∞) of cubic $SrTiO_3$ and $BaTiO_3$.

	$SrTiO_3$			$BaTiO_3$		
	Present	Present	Ref. [16]	Present	Present	Ref. [17]
a_{cell}	3.90[a]	4.01	3.92	3.90	4.01[a]	4.00
Z^* (Ti)	+7.11	+7.15	+7.56	+7.10	+7.14	+7.32
Z^* ($O_\parallel$)	−5.62	−5.71	−5.92	−5.62	−5.69	−5.78
Z^* (A)[b]	+2.30	+2.31	+2.55	+2.40	+2.37	+2.74
Z^* ($O_\perp$)	−1.89	−1.87	−2.12	−1.94	−1.91	−2.14
ε_∞	5.72	5.91	6.63	5.83	5.97	6.75
Expt. ε_∞^c	5.83	—	—	—	5.40	—

[a] Experimental lattice constants.
[b] Atom A represents strontium or barium.
[c] The experimental optical dielectric constants of $SrTiO_3$ and $BaTiO_3$ were taken from [36] and [37], respectively.

respectively), our results (5.72 and 5.97, FHI-PW92) are quite moderate.

The BECs (Z^*) of cubic $SrTiO_3$ and $BaTiO_3$ at experimental lattices (3.90 Å for $SrTiO_3$ and 4.01 Å for $BaTiO_3$) were calculated and are also presented in table 1, from which we can see that the amplitudes of Z^*(Ti) (+7.11 for $SrTiO_3$ and +7.14 for $BaTiO_3$) and the corresponding $Z^*(O_\parallel)$ (−5.62 for $SrTiO_3$ and −5.69 for $BaTiO_3$) substantially deviate from their nominal values expected in a purely ionic picture, i.e. +4 e and −2 e, respectively. This effect is indeed very common for the ABO_3 perovskite family [42, 43] and reflects the sensitivity of the covalent characteristics of the Ti–O bond to atomic displacements [17]. In contrast, Z^* (A) (A = Sr, Ba) and the corresponding $Z^*(O_\perp)$ are very close to their respective ionic charges, implying rather weak covalent characteristics of the Sr–O/Ba–O bonds.

To compare the BEC of $SrTiO_3$ with that of $BaTiO_3$ at the same lattice volume, we performed a computation for $SrTiO_3$ at the experimental lattice of $BaTiO_3$ (4.01 Å), and the results are also presented in table 1. With the substitution of Ba by Sr, however, the BECs of every atom of $SrTiO_3$ are almost identical with those of $BaTiO_3$. This insensitive change indicates that at the same lattice constant the long-range interaction of cubic $SrTiO_3$ is very similar to that of cubic $BaTiO_3$, which can also be confirmed in the following sections. Moreover, the compression of lattice volume only slightly affects the BECs of $SrTiO_3$—the calculated values differ by 0.10 e at most. Therefore it is expected that the long-range interaction is not responsible for the different phase transition behaviors of the two crystals.

3.2. *Effect of volume on the vibrational properties*

To investigate the effect of volume on vibrational properties, we computed the phonon dispersion relations of cubic $SrTiO_3$ and $BaTiO_3$ at different crystal volumes, and the results are depicted in figure 1. The unstable phonons, which are used to predict the phase transition behaviors of the compounds, are characterized by negative values. Moreover, to distinguish the contribution of each atom to the normalized eigenvector of a dynamical matrix, the points of the phonon bands are assigned by different colors (red for oxygen, blue for titanium, and green for strontium/barium).

It has been confirmed experimentally that $BaTiO_3$ undergoes a phase transition sequence from cubic symmetry to tetragonal, orthorhombic, and finally rhombohedral structures with decreasing temperature [3]. These transitions are all related to the congelation of a polar mode at the Γ point of the Brillouin zone. The results presented in figure 1(a) confirm the FE instability of cubic $BaTiO_3$ (a_0 = 4.01 Å), and it can be noted that the most unstable phonon dominated by the Ti and O displacements (in red and blue) is located at Γ point. Besides the Γ_{15} phonon, however, the Ti-dominated unstable branches also extend to other highly symmetrical points of Brillouin zone. Because the ΓX, ΓM, and ΓR lines correspond to the [100], [110], and [111] directions, respectively, the flat dispersions of the unstable ΓX and ΓM branches accompanied by the rapid frequency increase from Γ to R points indicate that the structural instabilities of cubic $BaTiO_3$ are restricted to three quasi two-dimensional 'planes' of reciprocal space intersecting at the Γ point. This typical characteristic thus reflects the 'chainlike' unstable localized distortions in real space [17]. Except for the aforementioned negative phonons, all other phonons are stable. The calculated phonon dispersion band of cubic $BaTiO_3$ at the experimental lattice (a_0 = 4.01 Å) is well consistent with previously

Table 2. Dielectric constants, equilibrium lattice constants, and Γ_{15} modes of cubic $BaTiO_3$ obtained by using different pseudopotentials and functionals.

Pseudopotential[a]	HGH			FHI			TM-NC
Functional[b]	TP	PW92	PBE	TP	PW92	PBE	TP
ε_∞^c	7.06	7.05	6.86	5.97	5.97	5.76	6.81
a_0 (Å)[d]	3.96	4.02	4.02	3.97	4.02	4.02	4.18
Γ_{15} mode (cm^{-1})[e]	−438	−438	−367	−162	−162	54	218

[a] Abbreviations for pseudopotentials: HGH, Hartwigsen–Goedeker–Hutter [39]; FHI, Fritz Haber Institute [29]; TM-NC, Troullier–Martins norm-conserving [28].
[b] Abbreviation for functionals: TP, Teter–Pade [40]; PW92, Perdew–Wang 92 [30]; PBE, Perdew–Burke–Ernzerhof [41].
[c] Theoretical optical dielectric constants obtained at the experimental lattice (a_0 = 4.01 Å).
[d] Optimized lattice constants obtained by using different pseudopotentials and functionals.
[e] Previous theoretical LDA and GGA values range from −72 to −219 cm^{-1} [10].

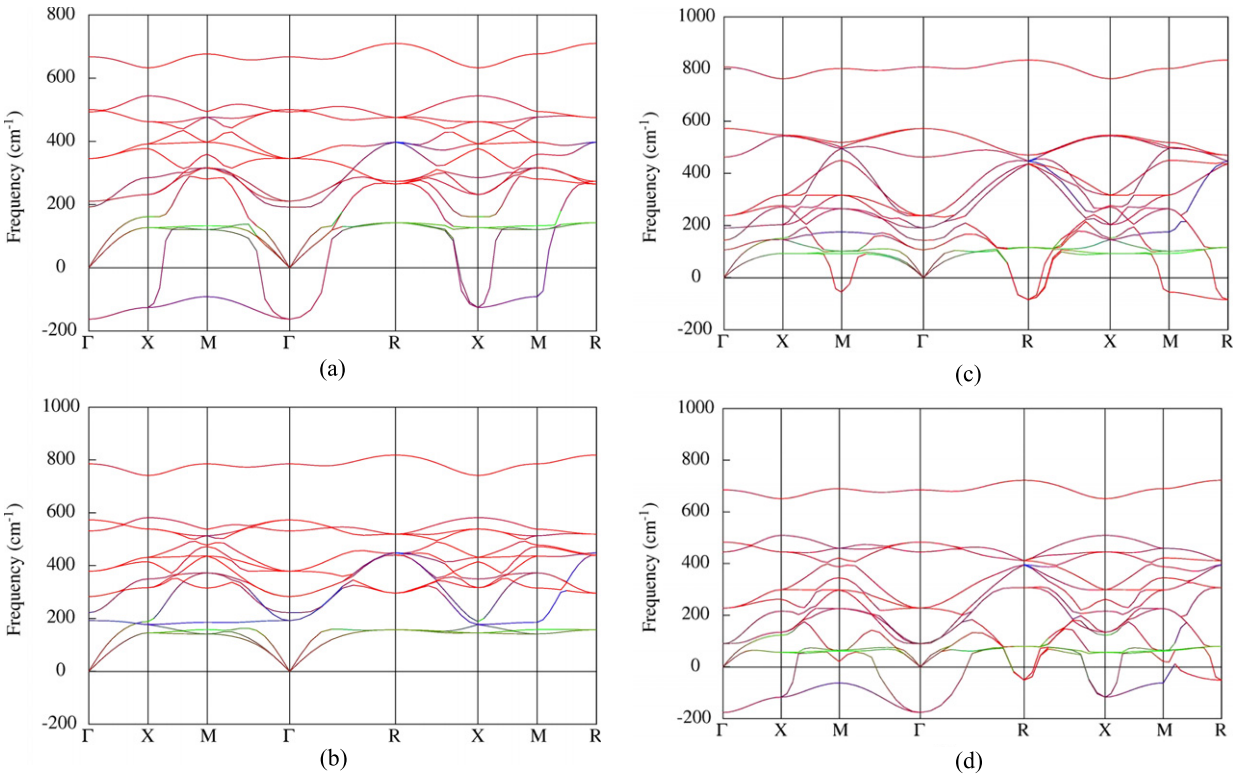

Figure 1. Phonon dispersion bands of $BaTiO_3$ and $SrTiO_3$ at different lattice constants: (a) $BaTiO_3$ at 4.01 Å (b) $BaTiO_3$ at 3.90 Å (c) $SrTiO_3$ at 3.90 Å (d) $SrTiO_3$ at 4.01 Å. Colors are assigned to each point according to the contribution of each atom to the dynamical matrix eigenvector (red for oxygen, blue for titanium, and green for Sr/Ba).

(This figure is in colour only in the electronic version)

published predictions [17, 44]. Moreover, with decreasing volume (a_0 = 3.90 Å) it can be noted from figure 1(b) that all the unstable ferroelectric phonons of cubic $BaTiO_3$ disappear. The result above is well consistent with the experimental observation that $BaTiO_3$ loses ferroelectricity at high pressure [45].

Figure 1(c) shows the phonon dispersion band of cubic $SrTiO_3$ at the experimental lattice (a_0 = 3.90 Å). The computational results indicate that the most unstable phonon found at the R point is triply degenerate and contains only the displacements of O atoms (in red). Because the R_{25} mode eigenvector can be characterized by the opposite rotations of oxygen octahedra in adjacent cells [16], the congelation of the R_{25} phonon thus leads to a tetragonal ($I_{4/mcm}$) structure, agreeing quite well with experimental observations [2]. Except for the R_{25} mode, an unstable phonon was also found at the M point of the Brillouin zone. This phonon, labeled as M_3, was reported to be temperature-independent through the AFD transition [16]. With the exception of the R_{25} and M_3 modes, no FE instabilities were found in cubic $SrTiO_3$ in the experimental lattice. The result is apparently different from previous theoretical investigations, in which an unstable Γ_{15} mode was found [16, 43]. According to experiments, the static dielectric response of $SrTiO_3$ above 50 K appears to obey the Curie–Weiss law, suggesting an impending FE transition at low temperatures [46]. However, $SrTiO_3$ does not turn into a FE phase but remains as a tetragonal ($I_{4/mcm}$) structure when the temperature approaches 0 K [46–48]. Further theoretical investigations also confirmed that the low temperature FE transition is completely suppressed because of so-called quantum paraelectric behavior [18, 49, 50].

Figure 1(d) depicts the phonon dispersion band of cubic $SrTiO_3$ at the experimental lattice of $BaTiO_3$ (a_0 = 4.01 Å). Because of the same lattice constant and symmetry, the Ti–O and A–O (A = Ba or Sr) distances in $SrTiO_3$ are equivalent with those of $BaTiO_3$. The differences in phonon bands thus reflect the changes of interaction caused by substitution. As can be seen from figures 1(a) and (d), an unstable R_{25} phonon appears along with the substitution of Ba by Sr, while the ΓX, ΓM, and XM unstable branches are almost identical in the two compounds. The results above suggest that the AFD instability is determined by the Sr–O interactions while the Ti–O interactions are crucial for the ΓX, ΓM, and XM unstable branches.

Since the unstable phonons are very important for elucidating the transition behaviors, we calculated the Γ_{15} and R_{25} modes of cubic $SrTiO_3$ and $BaTiO_3$ as a function of the lattice constant. As shown in figure 2, the Γ_{15} phonons in $BaTiO_3$ and $SrTiO_3$ keep the same variation trend and become unstable with increasing volume. The aforementioned trend is not only restricted to the present compounds but also appears in other perovskites. Samara and co-workers measured the pressure and temperature dependences of the dielectric properties of some antiferroelectric perovskites

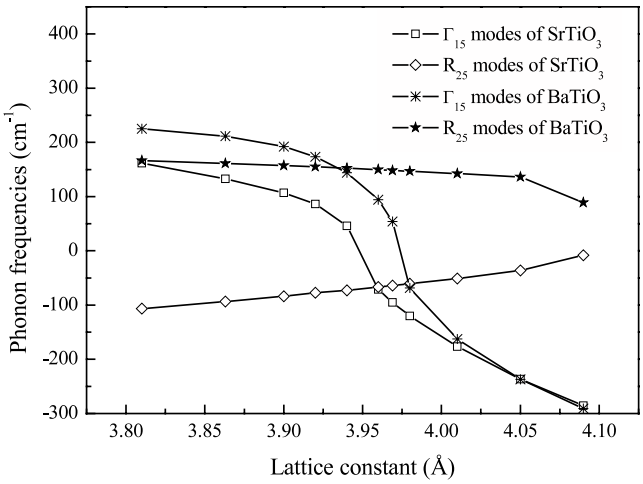

Figure 2. Γ_{15} and R_{25} phonons (cm^{-1}) of $BaTiO_3$ and $SrTiO_3$ as function of lattice constant (Å).

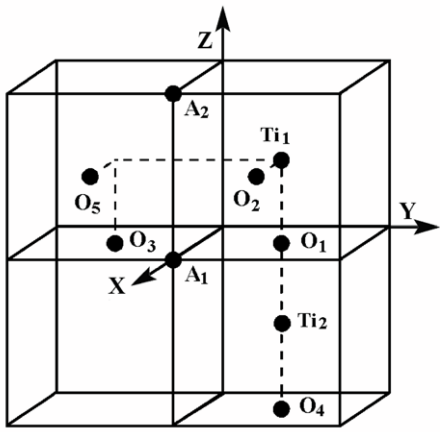

Figure 3. Three-dimensional view of atoms.

($PbZrO_3$, PbH_fO_3, and $BaMnF_4$) and confirmed that the FE transition temperature decreases with hydrostatic pressure [21, 22]. Moreover, Singh calculated the vibrational modes of $KNbO_3$ [23] while Fornari *et al* investigated the total energy dependence of rotational and ferroelectric lattice distortions in the $PbZr_xTi_{1-x}O_3$ system at different volumes [24]; both of their DFT results suggested that the Γ-point instability is enhanced with increasing volume [23, 24]. However, the behaviors of the R_{25} modes in $SrTiO_3$ and $BaTiO_3$ are completely different. In $SrTiO_3$, the unstable R_{25} phonon gradually becomes soft with decreasing volume. The opposite volume (pressure) dependence of FE and AFD instabilities in $SrTiO_3$ is similar to those in $PbZrO_3$, PbH_fO_3, $BaMnF_4$, and $PbZr_xTi_{1-x}O_3$ perovskites [21, 24], where the hydrostatic pressure can change the FE and AFE orderings in an opposite manner. But in $BaTiO_3$ no AFD instability can be found. The very different AFD behavior of $BaTiO_3$ compared with other perovskites seems related to its very large tolerance factor (1.0091 and 1.0706 for $SrTiO_3$ and $BaTiO_3$, respectively [51]), as emphasized by Ghita [20]. The results above are well consistent with previous experimental observations [2, 3, 21, 22] and theoretical predictions [23, 24, 52]. However, from a more fundamental viewpoint, the transition behavior of compounds is determined by the interactions of ionic pairs. Therefore, to figure out the origin of the different transition behaviors of cubic $SrTiO_3$ and $BaTiO_3$, further calculations concerning the interactions of each ionic pair are thus of primary importance (see section 3.3).

The discussions above concerning the FE and AFD behaviors of $SrTiO_3$ and $BaTiO_3$ were considered at low pressures (only 5% volume change). However, the perovskites may possess quite an unusual FE behavior at high pressure [53, 54]. From x-ray diffraction and high-pressure Raman scattering experiments, followed by some *ab initio* simulations, Kornev and co-workers confirmed that the ferroelectricity of $PbTiO_3$ disappears gradually with increasing pressure and then reappears as the pressure exceeds a critical point (above 30 GPa) [53]. Later, Bousquet and co-workers investigated the vibrational modes and interactions of cubic $BaTiO_3$ under hydrostatic pressures by first-principles calculations and also found that the FE instability of cubic $BaTiO_3$ reappears at about 140 GPa [54]. The abnormal behavior above cannot be observed in figure 1 because the volume compression in the present calculation (below 30 GPa) is not sufficiently large. However, our computations indicated at least that the low-pressure FE behaviors of $SrTiO_3$ and $BaTiO_3$ are quite consistent with previous results [53, 54]. In consideration of these facts, in next section we restrict ourselves to the changing interaction of each ionic pair at low pressure.

3.3. Origin of different transition behaviors of $BaTiO_3$ and $SrTiO_3$

In the sections above, some comparisons on the basis of the phonon bands between cubic $SrTiO_3$ and $BaTiO_3$ were made. In this section, the real-space IFCs, which are decomposed into a long-range DD part and a SR part according to [17] and [34], are employed to investigate the origin of their different transition behaviors. For convenience, the atoms are labeled according to figure 3 and the IFCs are reported either in Cartesian coordinates or in terms of the longitudinal (∥) and transverse (⊥) contributions along the line connecting the two atoms.

Table 3 lists the calculated IFCs of different ionic pairs of $BaTiO_3$ and $SrTiO_3$. For $BaTiO_3$, it has been confirmed that the unstable eigenvectors of the Γ_{15} phonon and the branches emanating from the Γ point are mainly dominated by Ti displacements along the Ti–O–Ti chain [7, 9, 17]. If only Ti atoms are allowed to be displaced, the energetics of the Ti-only displacement are thus determined by Ti self-force constant, Ti_1–Ti_2 longitudinal (∥) and transverse (⊥) interactions. Our calculations indicate that the total Ti_1–Ti_2 longitudinal (∥) interaction (−0.067) can compensate most of the Ti self-force constant (+0.1586), while the total Ti_1–Ti_2 transverse (⊥) interaction (+0.006) is very small. The above-calculated values are very similar to those of Ghosez, who suggested that the comparatively small Ti_1–Ti_2 transverse (⊥) interaction can directly account for the flat dispersion of the unstable ΓX and ΓM branches and the strong stiffening of the

Table 3. Longitudinal (∥), transverse (⊥), and Cartesian IFCs (hartree/bohr^2) between different pairs of atoms.

		$BaTiO_3$ (4.01 Å)			$SrTiO_3$ (4.01 Å)			$SrTiO_3$ (3.90 Å)		
Atom pair		Total	DD	SR	Total	DD	SR	Total	DD	SR
Ti_1–O_1	∥	+0.011	+0.250	−0.239	+0.007	+0.254	−0.247	−0.025	+0.279	−0.304
	⊥	−0.023	−0.042	+0.019	−0.023	−0.042	+0.018	−0.022	−0.047	+0.025
Ti_1–O_4	∥	+0.009	+0.009	0.000	+0.009	+0.009	0.000	+0.010	+0.010	0.000
	⊥	−0.002	−0.002	0.000	−0.002	−0.002	0.000	−0.002	−0.002	0.000
Ti_1–Ti_2	∥	−0.067	−0.039	−0.028	−0.067	−0.040	−0.027	−0.074	−0.044	−0.030
	⊥	+0.006	+0.020	−0.013	+0.007	+0.020	−0.014	+0.007	+0.022	−0.015
A_1–A_2	∥	−0.009	−0.004	−0.005	−0.008	−0.004	−0.004	−0.009	−0.005	−0.004
	⊥	+0.003	+0.002	+0.001	+0.003	+0.002	+0.001	+0.003	+0.002	+0.001
A_1–O_1	∥	−0.004	+0.007	−0.011	+0.007	+0.007	0.000	+0.006	+0.008	−0.002
	zz	−0.011	−0.015	+0.004	−0.011	−0.014	+0.003	−0.012	−0.016	+0.004
A_1–Ti_1	xx	+0.000	+0.000	−0.000	+0.000	+0.000	+0.000	+0.000	+0.000	+0.000
	xy	+0.012	+0.010	+0.002	+0.011	+0.010	+0.001	+0.013	+0.011	+0.020
	xz	+0.012	+0.010	+0.002	+0.011	+0.010	+0.001	+0.013	+0.011	+0.020

unstable ΓR branch [17]. However, for the true eigenvector, the contributions from the cooperative displacements are far from negligible. As can be noted from table 3, the largest DD (+0.250) and SR (−0.239) couplings are found in the longitudinal (∥) interactions of the Ti_1–O_1 pair. Because long-range characteristics predominate over the Ti_1–O_1 longitudinal (∥) interaction, the cooperative displacements of O_1 against Ti_1 along the Ti–O bond thus lead to a FE instability. This trend also provides an example of the very delicate nature of the compensation between DD and SR forces, as pointed out previously for $BaTiO_3$ [8, 55]. Besides the Ti_1–O_1 longitudinal (∥) interaction, the destabilizing nature of the Ti_1–O_4 longitudinal (∥) interaction also plays an important role in the FE instability. Together with the total contributions of the rest of the IFCs, the lattice dynamics and phase transition behaviors of cubic $BaTiO_3$ are thus determined.

For $SrTiO_3$ at expanded volume (a_0 = 4.01 Å), the Ti_1–Ti_2 longitudinal (∥) and transverse (⊥) interactions are almost the same as those in $BaTiO_3$. Also, the total longitudinal (∥) and transverse (⊥) interactions of the A_1–A_2, A_1–Ti_1, and Ti_1–O pairs were found to be very similar in the two compounds (table 3). The results confirm that the interactions above are responsible for the similar FE transition behaviors of $BaTiO_3$ and $SrTiO_3$. However, for the AFD phonons, the frequencies depend on the oxygen-related IFCs, self-force constants of oxygen, and off-diagonal couplings between neighboring O atoms. The present calculations suggest that at the same lattice constant the off-diagonal couplings of the O_1–O_2, O_1–O_3, O_1–O_4, or O_1–O_5 pairs of cubic $BaTiO_3$ and $SrTiO_3$ are remarkably similar to each other. The same conclusions can also be found in the cases of $BaTiO_3$, $PbTiO_3$, and $PbZrO_3$ [17]. Moreover, to identify which IFC is responsible for AFD instabilities, Ghosez and co-workers have artificially replaced the IFC between A_1 and O_1 atoms of $BaTiO_3$ by the values of $PbTiO_3$ and found that the R_{25} mode decreases from 125 to −40 cm^{-1} [17]. Furthermore, they also confirmed that the stronger A_1–O_1 interaction leads to a more unstable R_{25} mode [17]. Therefore, the effect of the A_1–O_1 interactions on AFD instability is confirmed. As shown in table 3, the A_1–O_1 interactions are indeed changed when Ba is substituted by Sr. The Ba–O_1 longitudinal (∥) interaction is repulsive (−0.004), while the Sr–O_1 longitudinal (∥) interaction (+0.007) possesses a long-range characteristic. Owing to the coordination number between Sr and O atoms (+0.007 × 12), the AFD instability is further reinforced. Although the change of the A_1–O_1 interaction can lead to a different AFD behavior, the role of the A–O interaction in $SrTiO_3$ is particularly different from other perovskites. On the basis of the first-principles calculations, Ghosez and co-workers investigated the lattice dynamics of $BaTiO_3$, $PbTiO_3$, and $PbZrO_3$ and confirmed that the covalent characteristics of Pb–O bonding result in a much larger BEC for Pb (+3.87) and a stronger A–O DD coupling (DD part of the A–O_1 longitudinal (∥) interaction, +0.016), which ultimately affect the transition behaviors (both FE and AFD instabilities) of $BaTiO_3$, $PbTiO_3$, and $PbZrO_3$ [17]. But for $SrTiO_3$, it can be noted from tables 1 and 2 that the long-range DD couplings of all ionic pairs as well as the BEC of atom A in $SrTiO_3$ are quite similar to those of $BaTiO_3$, suggesting that at the same lattice volume the polarization of the system is hardly affected by the substitution. Moreover, as already identified in figures 1(a) and (d), the contributions of Sr/Ba displacements to the unstable FE phonon branches are nearly identical. In consideration of similar valence configurations, $5s^25p^66s^2$ for Ba and $4s^24p^65s^2$ for Sr, the covalent effect of A–O bond on the lattice dynamics of $BaTiO_3$ and $SrTiO_3$ is thus exclusive. Furthermore, it can be confirmed that the different A_1–O_1 longitudinal (∥) interactions of $BaTiO_3$ and $SrTiO_3$ are due to the SR coupling (table 3) but not the DD part. Because the SR repulsion (−0.011) of the A_1–O_1 longitudinal (∥) interaction in $BaTiO_3$ is much stronger than that (0.000) in $SrTiO_3$, consistent with the larger ionic radius of Ba (1.61 Å) than Sr (1.44 Å) [56], it can be deduced that the ionic radius of atom A is very crucial for the different AFD behaviors of $ATiO_3$ (A = Ba, Sr) perovskites.

The IFCs of $SrTiO_3$ at the experimental lattice (a_0 = 3.90 Å) presented in table 3 indicate that the Ti_1–O_1 longitudinal (∥) interaction (−0.025) is changed and becomes repulsive with decreasing volume while other IFCs are rather insensitive to lattice change. As the destabilizing nature of the Ti_1–O_4 longitudinal (∥) interaction (+0.010) is no longer sufficient to compensate the Ti_1–O_1 repulsion, the FE

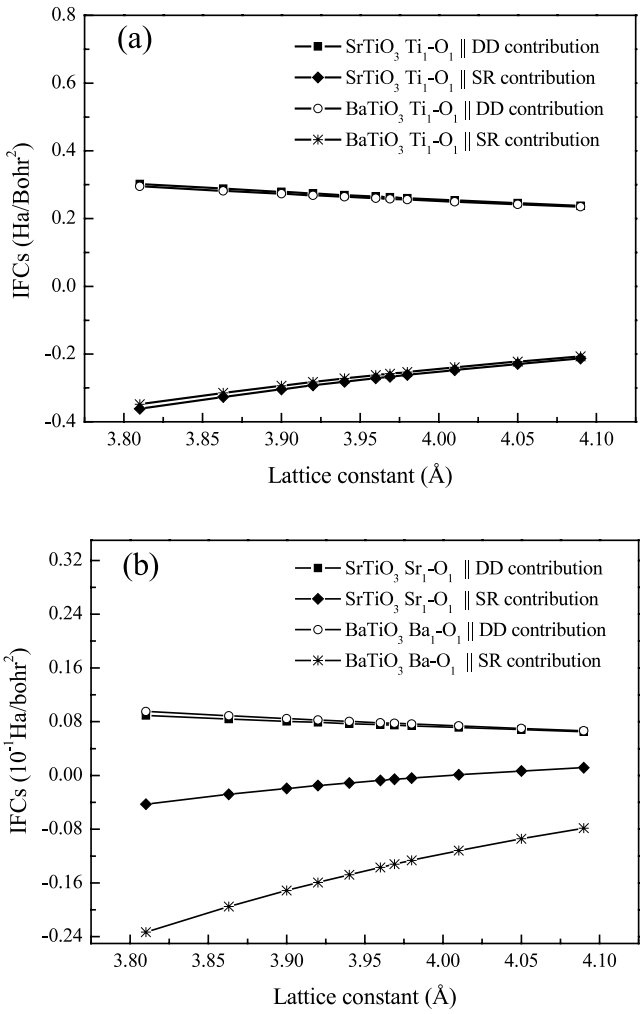

Figure 4. Key IFCs (Ha/Bohr^2) for $BaTiO_3$ and $SrTiO_3$ as a function of lattice constant (Å).

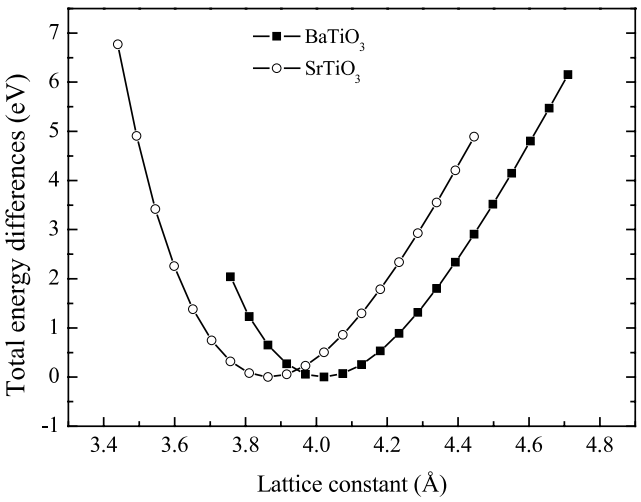

Figure 5. Total energy differences (eV) as a function of lattice constant (Å) in $BaTiO_3$ and $SrTiO_3$. The energy zero points are taken from the total energies of corresponding equilibrium configurations.

instabilities thus disappear. To identify the effect of change of crystal volume on lattice dynamics, we calculated the IFCs of $BaTiO_3$ and $SrTiO_3$ at a number of volumes. The key IFCs as a function of lattice constant are depicted in figure 4. It can be found from figure 4(a) that the long-range DD interactions or SR repulsions of the Ti_1–O_1 pairs of $BaTiO_3$ and $SrTiO_3$ are very close to each other. With decreasing volume, the SR repulsion gradually becomes dominant over the long-range interaction, leading to a stiffening of the Γ_{15} phonon and the disappearance of the FE instabilities. These results agree quite well with the trend of the Γ_{15} modes of $BaTiO_3$ and $SrTiO_3$ observed in figure 2 and tie in with previous theoretical predictions that increasing crystal volume can enhance FE instability [7, 11, 23]. Figure 4(b) shows the DD and SR interactions of the A_1–O_1 pairs of $BaTiO_3$ and $SrTiO_3$. At the same crystal volume, the long-range interactions in the two compounds are very similar to each other, being consistent with the calculated BECs of the two compounds. For $BaTiO_3$, the magnitude of the SR repulsion is much larger than the long-range DD interaction, and therefore no AFD instability can be produced. However, owing to the smaller ionic radius of Sr relative to Ba, the repulsion between Sr and O atoms is significantly weakened, and the long-range characteristic of the Sr–O pair thus leads to an AFD R_{25} phonon of $SrTiO_3$.

Beside the A–O interactions, the different ionic radii of Sr and Ba can also result in different ground-state configurations. Figure 5 depicts the total energies of cubic $BaTiO_3$ and $SrTiO_3$ as function of lattice constant. The equilibrium lattice constants of $BaTiO_3$ and $SrTiO_3$ are optimized to be 4.02 Å and 3.86 Å, respectively, being in good agreement with the experimental values [9]. As shown in figure 5, when the lattice constant deceases from 4.02 to 3.86 Å, the total energy of $BaTiO_3$ gradually increases. This is opposite to the case in $SrTiO_3$. The different total energy dependence of volume can be attributed to the interactions of the A–O and Ti–O pairs. For $BaTiO_3$, the repulsions of both the Ti–O and Ba–O pairs are enhanced with decreasing volume, being consistent with the increase in total energy. However, for $SrTiO_3$ the interactions of the Sr–O pairs are attractive, and the increasing repulsion between Ti and O atoms with decreasing volume (from 4.02 to 3.86 Å) does not lead to an increase of total energy owing to the compensated Sr–O interaction. As a result, the lattice constant of $SrTiO_3$ can be significantly reduced, which distinguishes the FE behavior of $SrTiO_3$ from $BaTiO_3$. As a result, it can be concluded that the smaller ionic radius of Sr compared with Ba, which essentially leads to different SR couplings of A–O pairs, is not only crucial for the very different AFD behaviors but also for the different lattice constants of the two compounds. The substitution and different lattice constants make the transition behaviors of the two compounds entirely different.

4. Conclusions

Using first-principles DFT calculations, we have systematically investigated the lattice dynamics of cubic $BaTiO_3$ and $SrTiO_3$ as a function of crystal volume. The phonon dispersion relations of the two compounds identify their different phase transition behaviors. From real-space analysis, it can be found that these differences can be elucidated by a few key

IFCs. First, the Ti–O interaction is very crucial for the FE Γ_{15} modes and unstable phonon branches emanating from the Γ point. As the lattice constant decreases, the repulsion of the Ti–O pair becomes dominant over the Ti–O interaction, which results in the disappearance of the FE instabilities. Second, the A–O interactions in the two compounds are very different. For $SrTiO_3$, the Sr–O interaction is governed by long-range characteristics. However, for $BaTiO_3$, the Ba–O interaction is repulsive. The different A–O interactions result in a very different AFD behavior. Different from $PbTiO_3$ and $PbZrO_3$, the appearance of the AFD R_{25} mode in $SrTiO_3$ does not originate from the characteristics of the covalent bonding between A and O atoms but relates to the A–O SR coupling. Because the A–O SR couplings are closely related to ionic radius, it can be confirmed that the smaller ionic radius of Sr (1.44 Å) relative to Ba (1.61 Å) is crucial for the very different AFD behaviors of $BaTiO_3$ and $SrTiO_3$. Finally, owing to the compensated Sr–O interaction, the increasing repulsion between Ti and O atoms of $SrTiO_3$ with decreasing volume (from 4.02 to 3.86 Å) does not result in an increase in total energy. Therefore, the lattice constant of $SrTiO_3$ can be significantly reduced, which results in the different FE behaviors of the two compounds. The substitution and difference in crystal volume make the phase transitions of the two compounds entirely different.

Acknowledgments

This work was supported by the Key Program Projects of National Natural Science Foundation of China (20431030), National Natural Science Foundation of China (20671032), and Program for New Century Excellent Talents in University of China (NCET-04-0341).

References

[1] Lines M E and Glass A M 1977 *Principles and Applications of Ferroelectrics and Related Materials* (Oxford: Clarendon)
[2] Fleury P A, Scott J F and Worlock J M 1968 *Phys. Rev. Lett.* **21** 16
[3] Perry C H and Hall D B 1965 *Phys. Rev. Lett.* **15** 700
[4] Cardona M 1965 *Phys. Rev.* **140** A651
[5] Vogt H 1995 *Phys. Rev.* B **51** 8046
[6] DiDomenico M, Porto S P S and Wemple S H 1967 *Phys. Rev. Lett.* **19** 855
[7] Cohen R E and Krakauer H 1990 *Phys. Rev.* B **42** 6416
[8] Cohen R E 1992 *Nature* **358** 136
[9] King-Smith R D and Vanderbilt D 1994 *Phys. Rev.* B **49** 5828
[10] Chen Z X, Chen Y and Jiang Y S 2001 *J. Phys. Chem.* B **105** 5766
[11] Zhong W and Vanderbilt D 1995 *Phys. Rev. Lett.* **74** 2587
[12] Zhong W, Vanderbilt D and Rabe K M 1994 *Phys. Rev. Lett.* **73** 1861
[13] Zhong W, Vanderbilt D and Rabe K M 1995 *Phys. Rev.* B **52** 6301
[14] Rabe K M and Wagmare U V 1996 *J. Phys. Chem. Solids* **57** 1397
[15] Baroni S, de Gironcoli S, Corso A D and Giannozzi P 2001 *Rev. Mod. Phys.* **73** 515
[16] Lasota C, Wang C Z, Yu R and Krakauer H 1997 *Ferroelectrics* **194** 109
[17] Ghosez Ph, Cockayne E, Waghmare U V and Rabe K M 1999 *Phys. Rev.* B **60** 836
[18] Trautmann Th and Falter C 2004 *J. Phys.: Condens. Matter* **16** 5955
[19] Piskunov S, Heifets E, Eglitis R I and Borstel G 2004 *Comput. Mater. Sci.* **29** 165
[20] Ghita M, Fornari M, Singh D J and Halilov S V 2005 *Phys. Rev.* B **72** 054114
[21] Samara G A 1970 *Phys. Rev.* B **1** 3777
[22] Samara G A, Sakudo T and Yoshimitsu K 1975 *Phys. Rev. Lett.* **35** 1767
[23] Singh D J and Boyer L L 1992 *Ferroelectrics* **136** 95
[24] Fornari M and Singh D J 2001 *Phys. Rev.* B **63** 092101
[25] Hohenberg P and Kohn W 1964 *Phys. Rev.* **136** B864
[26] Gonze X, Beuken J M, Caracas R, Detraux F, Fuchs M, Rignanese G M, Sindic L, Verstraete M, Zerah G, Jollet F, Torrent M, Roy A, Mikami M, Ghosez Ph, Raty J Y and Allan D C 2002 *Comput. Mater. Sci.* **25** 478
[27] Gonze X, Rignanese G M, Verstraete M, Beuken J M, Pouillon Y, Caracas R, Jollet F, Torrent M, Zerah G, Mikami M, Ghosez Ph, Veithen M, Raty J Y, Olevano V, Bruneval F, Reining L, Godby R, Onida G, Hamman D R and Allan D C 2005 *Z. Kristallogr.* **220** 558
[28] Troullier N and Martins J L 1991 *Phys. Rev.* B **43** 1993
[29] Fuchs M and Scheffler M 1999 *Comput. Phys. Commun.* **119** 67
[30] Perdew J P and Wang Y 1992 *Phys. Rev.* B **45** 13244
[31] Ceperley D M and Alder B J 1980 *Phys. Rev. Lett.* **45** 566
[32] Gonze X 1996 *Phys. Rev.* B **54** 4383
[33] Monkhorst H J and Pack J D 1976 *Phys. Rev.* B **13** 5188
[34] Gonze X, Charlier J C, Allan D C and Teter M P 1994 *Phys. Rev.* B **50** 13035
[35] Giannozzi P, de Gironcoli S, Pavone P and Baroni S 1991 *Phys. Rev.* B **43** 7231
[36] Dore P, Paolone A and Trippetti R 1996 *J. Appl. Phys.* **80** 5270
[37] Burns G and Dacol F H 1982 *Solid State Commun.* **42** 9
[38] Gonze X, Ghosez Ph and Godby R W 1995 *Phys. Rev. Lett.* **74** 4035
[39] Hartwigsen C, Goedecker S and Hutter J 1998 *Phys. Rev.* B **58** 3641
[40] Goedecker S, Teter M and Huetter J 1996 *Phys. Rev.* B **54** 1703
[41] Perdew J P, Burke K and Ernzerhof M 1996 *Phys. Rev. Lett.* **77** 3865
[42] Ghosez Ph, Michenaud J P and Gonze X 1998 *Phys. Rev.* B **58** 6224
[43] Zhong W, King-Smith R D and Vanderbilt D 1994 *Phys. Rev. Lett.* **72** 3618
[44] Ghosez Ph, Gonze X and Michenaud J P 1998 *Ferroelectrics* **206** 205
[45] Decker D L and Zhao Y X 1989 *Phys. Rev.* B **39** 2432
[46] Viana R, Lunkenheimer P, Hemberger J, Böhmer R and Loidl A 1994 *Phys. Rev.* B **50** 601
[47] Sakudo T and Unoki H 1971 *Phys. Rev. Lett.* **26** 851
[48] Müller K A and Burkard H 1979 *Phys. Rev.* B **19** 3593
[49] Martoňák R and Tosatti E 1994 *Phys. Rev.* B **49** 12596
[50] Zhong W and Vanderbilt D 1996 *Phys. Rev.* B **53** 5047
[51] Goudochnikov P and Bell A J 2007 *J. Phys.: Condens. Matter* **19** 176201
[52] Xie Y, Fu H G, Yu H T, Zhang G X and Sun J Z 2007 *J. Phys.: Condens. Matter* **19** 506213
[53] Kornev I A, Bellaiche L, Bouvier P, Janolin P E, Dkhil B and Kreisel J 2005 *Phys. Rev. Lett.* **95** 196804
[54] Bousquet E and Ghosez Ph 2006 *Phys. Rev.* B **74** 180101
[55] Ghosez Ph, Gonze X and Michenaud J P 1996 *Europhys. Lett.* **33** 713
[56] Lide D R 2003 *CRC Handbook of Chemistry and Physics* 84th edn (Boca Raton, FL: CRC Press) p 1959